MODELING OF CASTING, WELDING, AND ADVANCED SOLIDIFICATION PROCESSES – XII

We wish to thank Magma for sponsoring this proceedings volume for
Modeling of Casting, Welding, and Advanced Solidification Processes – XII

MODELING OF CASTING, WELDING, AND ADVANCED SOLIDIFICATION PROCESSES - XII

Related titles include:

- *Shape Casting: Third International Symposium*
- *Modeling of Casting, Welding, and Advanced Solidification XI (CD-ROM)*
- *Frontiers in Solidification Science*

HOW TO ORDER PUBLICATIONS

For a complete listing of TMS publications, contact TMS at (724) 776-9000 or (800) 759-4TMS or visit the TMS Knowledge Resource Center at http://knowledge.tms.org:

- Purchase publications conveniently online and download electronic publications instantly.
- View complete descriptions and tables of contents.
- Find award-winning landmark papers and webcasts.

MEMBER DISCOUNTS

TMS members receive a 30 percent discount on TMS publications. In addition, members receive a free subscription to the monthly technical journal *JOM* (both in print and online), free downloads from the Materials Technology@TMS digital resource center (www.materialstechnology.org), discounts on meeting registrations, and additional online resources to name a few of the benefits. To begin saving immediately on TMS publications, complete a membership application when placing your order or contact TMS:

Telephone: (724) 776-9000 / (800) 759-4TMS

E-mail: membership@tms.org or publications@tms.org

Web: www.tms.org

Modeling of Casting, Welding, and Advanced Solidification Processes - XII
Edited by: Steve L. Cockcroft and Daan M. Maijer
TMS (The Minerals, Metals & Materials Society), 2009

MICRO-MACROSEGREGATION PREDICTION BASED ON SOLIDIFICATION SIMULATION FOR CONTINUOUS CASTING OF TERNARY BRONZE ALLOYS

M. Grasser[1], A. Ishmurzin[1], F. Mayer[1], M. Wu[1], A. Ludwig[1], U. Hofmann[2], J. Riedle[2]

[1]Christian-Doppler Laboratory for Multiphase Modeling of Metallurgical Processes
Dept. of Metallurgy, University of Leoben, A-8700, Austria
[2]Wieland Werke AG Ulm, Vöhringen, Germany

Keywords: thermodynamics; ternary; solidification; macrosegregation

Abstract

The paper discusses simulation results for columnar solidification of ternary bronze in continuous casting of round blooms. The thermodynamics of the system Cu-Sn-P is included (i) by applying linearized phase diagram information for solidification processes with and without considering feeding induced flow; (ii) by taking into account the existence of peritectic grooves by applying splines to approximate the liquidus temperature and the solubility of Sn and P in the different solidifying solids. The volume-averaging solidification model considers two interpenetrating continua, i.e. the melt as the primary phase and columnar dendrites as the secondary phase. At the interface, it is distinguished explicitly between interface and average concentrations. The formation of columnar dendrites is approximated by growing cylinders. After their formation at the mold/metal interface, they are considered to move continuously with the applied casting speed. The velocity field of the melt flow is obtained by solving the momentum conservation equation. Within the mushy zone we consider hydrodynamic interaction between melt and solid and local formation of microsegregation. A comparison of the simulated liquid and solid concentration with corresponding ternary Scheil calculations is given and discussed. In addition the comparison of the average mixture concentration of the simulation results with experimental concentration measurements indicate similar tendencies for macrosegregation.

Introduction

Since technical alloys usually consist of more than two elements, macrosegregation studies imply the need of taking thermodynamics for ternary or higher order systems into account. Fig. 1 shows a typical microstructure observed in vertical continuous casting of bronze just after casting without any heat treatment. On the left side, the phase distribution at an outer boundary is shown whereas on the right the microstructure in the centre of the casting is displayed. The location of both micrographs is indicated schematically in the middle part of Fig. 1. It is obvious that the microstructure at the centre is finer with less α-δ eutectoid compared to the outer boundary region. Measurements reveal that the tin content at the outer boundary is the highest and gradually decreased towards the centre. This concentration inhomogeneity is often referred to as macrosegregation. Fig. 2 shows such a profile as measured by industry. Since it is not possible to remove macroscopic concentration inhomogeneity by heat treatment, it is of great importance to reduce, if possible, their formation directly during casting.

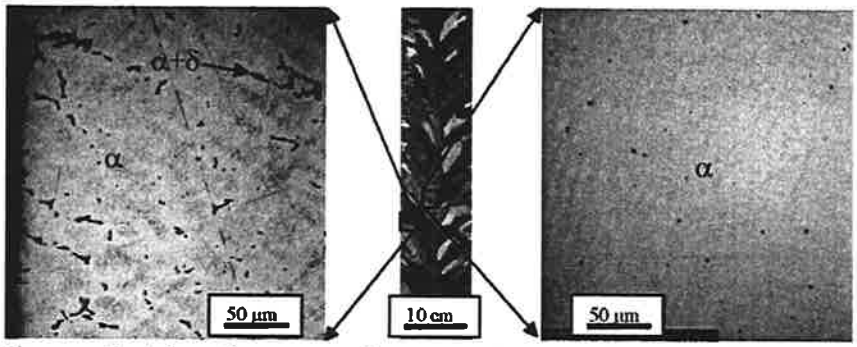

Figure 1. Micrographs taken from a continuous casting strand of CuSn8P0.005 bronze. Left: microstructure at the outer boundary. Dark regions show eutectoid structure where the rigid α-δ eutectoid is present. Middle: columnar grain structure; rectangles: schematic position of the two micrographs left and right. Right: microstructure in the centre, here the microstructure is more homogeneous than at the outer boundary because almost no eutectoid is present.

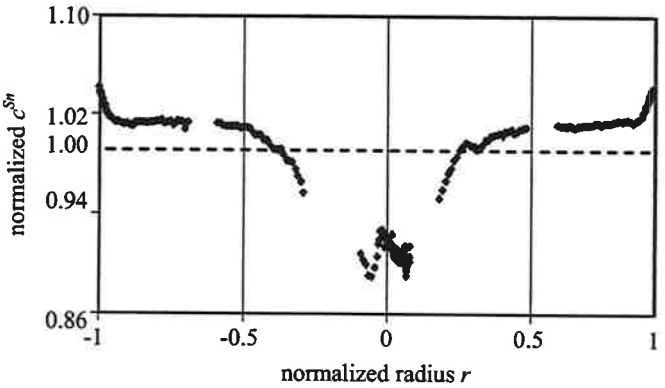

Figure 2. Normalized macrosegregation profile of Sn for a round bloom (CuSn7.6P0.022 alloy). Positive macrosegregation is obtained at the surface and negative one at the center [1].

Since the pioneer work of Kaufman and Bernstein in 1970 [2], calculations of phase diagrams have become a widely used tool for predicting thermodynamic information by computational techniques. This method, known as the CALPHAD method (CALculation of PHAse Diagrams) [3,4], enables the prediction of phase evolution and of corresponding solidification paths by taking into account different cooling rates, back diffusion, and/or coarsening [5,6,7]. During the last years it was tried to improve the accuracy of macrosegregation prediction in continuous casting of non-ferrous alloys by including thermodynamics of higher order systems. For example Eskin [8] discussed the formation of segregation for a ternary Al-alloy based on a two phase model for equiaxed solidification. He stated that direct coupling between thermodynamic calculations and CFD simulations might be rather time consuming, especially if an industrial size casting process is considered. Besides, improvements were done to numerically describe the formation of macrosegregation in continuous casting of bronze [9,10,11]. To model such a solidification process, conservation equations for mass, enthalpy, and solute were considered on the macroscopic scale and thermodynamic equilibrium conditions on the liquid/solid interfacial microscale. Ludwig and co-workers proposed a method [10,11] to couple thermodynamic data with a multiphase solidification model. Since direct coupling is rather time consuming, the coupling is done by providing access to thermodynamic data through linearization methods, splines or tabulation and interpolation techniques like ISAT (In-Situ Adaptive Tabulation) [12].

Model

During solidification of continuous casting of bronze, equiaxed or/and columnar dendritic growth is observed depending on the applied casting conditions. A multiphase model for columnar and/or equiaxed solidification has been developed by Ludwig, Wu, and co-workers from 2002-2007 [13-16]. For the simulations discussed in the present paper this model was applied, whereat nucleation and growth of equiaxed grains were neglected. The thermodynamic information of Cu-Sn-P as published in [10-12] is included by coupling pre-calculated thermodynamic data with the multiphase model. In Case AI and Case AII (case definition see below) linearized phase diagram data and in Case B splines of third order were used to model thermodynamics during solidification. In Case AII and Case B feeding flow is included by taking the density difference between solid and liquid ($\rho_c > \rho_l$) into account. Since earlier simulations for the binary bronze (CuSn6) showed that feeding flow dominated the formation of macrosegregation, thermo-solutal convection was neglected here.

Geometry, Boundary Conditions, and Thermodynamic Data

For the present macrosegregation study a cylindrical mold was used and thus 2D axis-symmetrical conditions were assumed. Geometry, boundary conditions, and numerical settings are described in detail in [9]. For the process simulation a casting velocity of $\vec{u}_{cast} = 1.92$ mm·s^{-1} and a casting temperature of $T_{cast} = 1389$ K were taken. The grid consisted of 9296 square cells. As initial condition, hot melt ($T_{init} = 1297$ K) was considered for the whole casting. Calculations were done for the ternary alloy CuSn6P0.5. Fig. 3 shows the geometry applied for all three cases together with the steady-state temperature distribution obtained for Case AII.

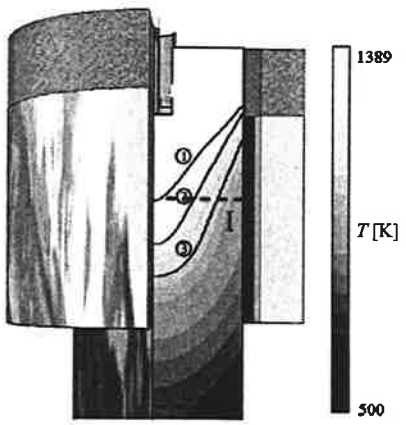

Figure 3: Simulated steady-state temperature distribution in the continuous casting round strand for the ternary alloy CuSn6P0.5 where feeding and inlet flow were considered (Case AII). Black lines: (①) liquid temperature $T_L^0 = 1295.5$ K, (②) volume fraction columnar phase $f_c = 0.5$ and (③) $f_c = 0.83$. At line I and II concentration predictions are analyzed.

Fig. 4 shows the liquidus surface of the Cu rich corner of the ternary phase diagram for Cu-Sn-P (based on calculations with Thermo-Calc) including different monovariant lines. In the calculation with the multiphase solidification code, the liquidus surface, T_L, and the concentration of the two alloying elements in the solid at the solid/liquid interface, $\tilde{c}_c^{Sn}$ and $\tilde{c}_c^{P}$, are based on computational thermodynamics (Thermo-Calc). For the industrial application of the model these three thermodynamic functions are linearized around the initial alloy composition A for Case AI and Case AII and spline-interpolated over the whole area in Case B [12]. In general, solidification of bronze alloys starts with the formation of α dendrites. The black arrows in Fig. 3 indicate the solidification path of CuSn6P0.5 schematically. The point A indicates the

initial alloy concentration whereas point B the end of solidification according to a ternary Scheil-calculation. During primary solidification the melt enriches and so the solidification path crosses the first peritectic groove at P_1. Between P_1 and the second peritectic groove P_2 the melt forms β and between P_2 and the eutectic groove E the melt form γ. In the eutectic groove E two binary eutectics form first γ + Cu_3P and later α + Cu_3P. As soon as the concentration of the remaining melt fits to a concentration that occurs in the eutectic groove, the binary eutectics forms, and the melt concentration follows the eutectic groove until it reaches the ternary eutectic point (B). There, the formation of the ternary eutectic α + Cu_3P + β terminates the solidification process finally. Note that if back diffusion in the solid phases (α, β, γ) is significant, the solidification path may not reach the ternary eutectic point (B). And note that due to a larger solubility of Sn in β and γ, the solidification path turns at point P_1 towards lower Sn concentrations.

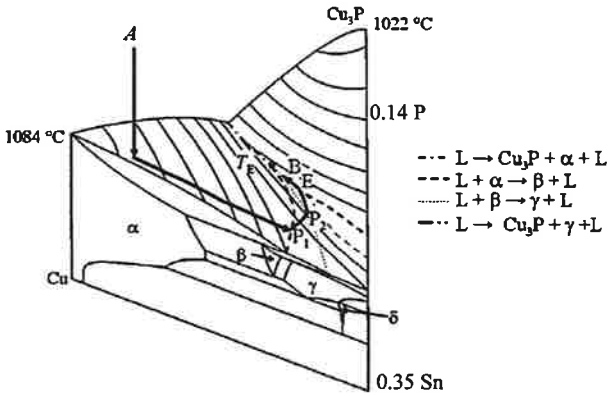

Figure 4: 3D liquidus surface with isotherms for the ternary phase diagram Cu-Sn-P in the Cu rich corner up to 0.35 mass fraction Sn and 0.14 mass fraction P (based on calculations with Thermo-Calc, database CuSnII). Broken lines: monovariant lines of the liquidus surface; front view: binary phase diagram of Cu-Sn; black arrows: solidification path of an alloy with concentration *A* (CuSn6P0.5) according to the Thermo-Calc Scheil model; P_1: first peritectic groove, P_2: second peritectic groove, E: eutectic groove, B: end of solidification. T_E: ternary eutectic point. The phases labeled in the figures are α = Cu (max. Sn 15.8 wt.%); β ~ $Cu_{17}Sn_3$; γ ~ Cu_3Sn; δ ~ $Cu_{41}Sn_{11}$ [17].

Results and Discussion

Ternary Calculation with Linear Interpolation Functions (Case AI)

In Case AI one set of linear interpolation functions around the alloy concentration *A* is applied to described the liquids temperature, T_L, and the solubility of Sn and P in the primary, columnar α-phase, $\tilde{c}_c^{Sn}$, and $\tilde{c}_c^{P}$. So Case AI neglects the appearance of the first peritectic groove at point P_1 (and all other grooves). With this simplified thermodynamics, process simulations according to Fig. 3 were done. As feeding flow and thermo-solutal flow are neglected for Case AI, and the inlet flow does not lead to strong relative motion between the liquid and solid, no macrosegregation will form in this case. In Fig. 5 the predicted liquid enrichment for Sn and P is shown in comparison with a ternary Scheil calculation done with Thermo-Calc. The curves were taken perpendicular to the casting direction along the line labeled with I in Fig. 3. It is obvious that the single set the linear interpolation functions is only suitable for solid fractions less than 60 %, especially with respect to Sn enrichment. As the solubility of P for the different solid phases is comparable, the melt enrichment with P is well described with the simple "linear" thermodynamics even above a solid fraction of 60 %. The applied multiphase model for columnar solidification assumes a shell wise growth of cylinders to approximate growing columnar dendrites. The "solid" concentrations within a corresponding control volume element, $\bar{c}_c^{Sn}$ and $\bar{c}_c^{P}$, reflects the average concentrations of the solid which has form in that particular

volume element so far. For a comparison with a ternary Scheil calculation, the corresponding solid concentrations at the solid/liquid interface are cumulated according to

$$\bar{c}_c^{Scheil,i} = \frac{1}{f_c}\sum c_c^{Scheil,i}\Delta f_c^{Scheil}, \text{ where } i = \text{Sn, P.} \quad (1)$$

Here, $c_c^{Scheil,i}$ is the solid concentration at the solid/liquid interface for element i and Δf_c^{Scheil} the change in the solid volume fraction according to the ternary Thermo-Calc Scheil calculation.

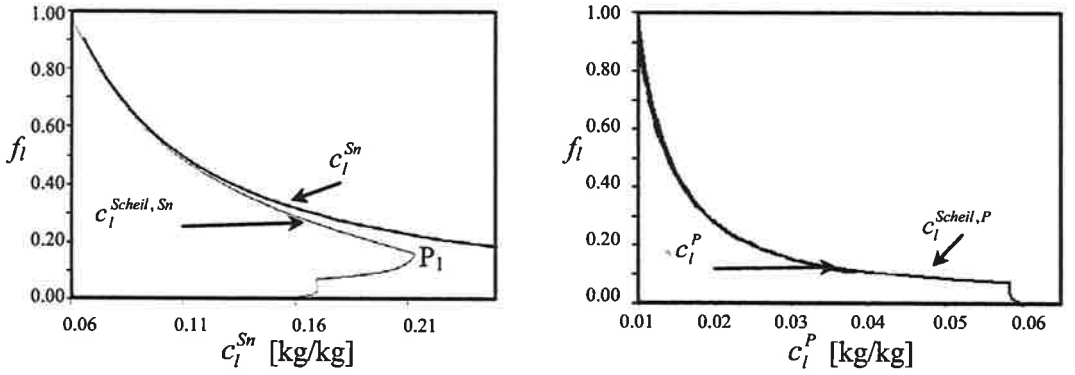

Figure 4: Scheil curve calculated based on Thermo-Calc (database CuSnII, gray line) compared to the liquid concentration of the FLUENT calculation for CuSn6P0.5 (black line) versus f_l (a) $c_l^{Scheil,Sn}$ and c_l^{Sn}, (b) $c_l^{Scheil,P}$ and c_l^{P}.

in the simulation for lower liquid volume fractions due to the fact that the tin rich phases are not considered. However, $\bar{c}_c^{P}$ is close to that predicted by Scheil calculations down to $f_l < 0.1$.

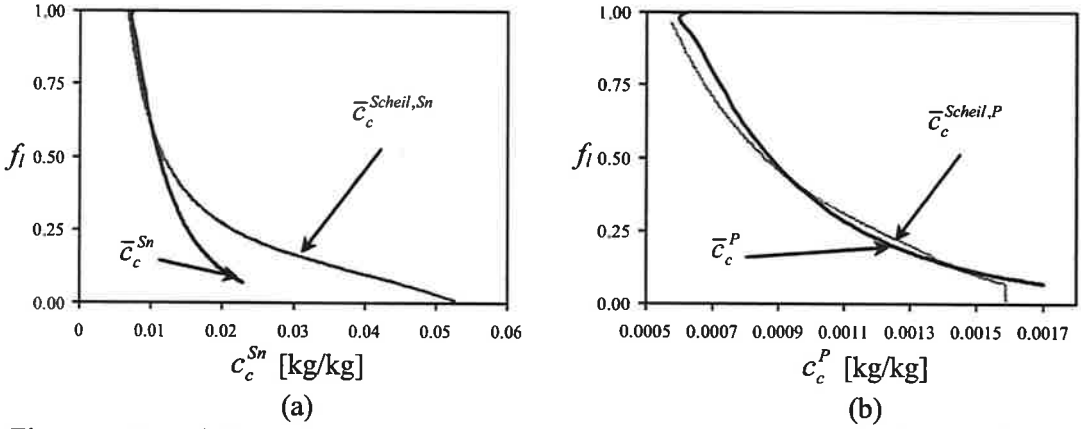

Figure 5: Cumulative Scheil curve calculated based on Thermo-Calc (database CuSnII, gray line) compared to the columnar concentration of the FLUENT calculation for CuSn6P0.5 (black line) versus f_c (a) $\bar{c}_c^{Scheil,Sn}$ and $\bar{c}_c^{Sn}$, (b) $\bar{c}_c^{Scheil,P}$ and $\bar{c}_c^{P}$.

Fig. 6 shows liquid fraction f_l versus $\bar{c}_c^{i}$ and $\bar{c}_c^{Scheil,i}$ for Sn and P calculated for CuSn6P0.5 ($f_l - \bar{c}_c^{i}$ taken along line I, Fig. 2). For Sn the cumulated Scheil curve and the averaged solid concentration $\bar{c}_c^{Sn}$ do not differ significantly until $f_l \leq 0.5$. After that limit the linear approximation for the liquids temperature, T_L, and the solubility of Sn and P in the primary, columnar α-phase, $\tilde{c}_c^{Sn}$, and $\tilde{c}_c^{P}$ is a poor approximation. For P the deviation between cumulated Scheil and averaged solid concentration is less pronounced. As mentioned above, this is due to the comparable solubility of P for the different solid phases.

Comparison of Simulation Results of Case AII with Experimental Data

In order to study macrosegregation quantitatively a mixture concentration c^i_{mix} is defined according to [15]

$$c^i_{mix} = \frac{c^i_l \rho_l f_l + c^i_c \rho_c f_c}{\rho_l f_l + \rho_c f_c}, \text{ where } i = \text{Sn, P} \qquad (2)$$

Here, c^i_c is the cumulative columnar concentration corresponding to the shell wise growth during solidification, c^i_l the corresponding concentration in the liquid, f_l and f_c volume fraction of liquid and columnar solid phase, and ρ_l and ρ_c the corresponding densities. In Fig. 7 the c^{Sn}_{mix}- and c^P_{mix}- distribution is shown as calculated. Here, the predicted normalized macrosegregation profiles for Sn and P are plotted for a cross section close to the outlet (at line II, Fig. 3) for the case where linearized ternary thermodynamic information are applied together with feeding flow (Case AII).

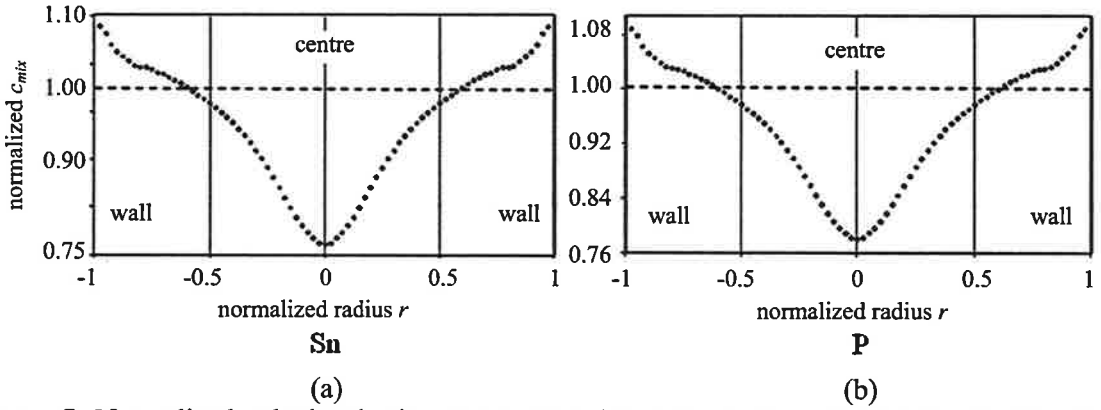

Figure 7: Normalized calculated mixture concentration close to the outlet (at line II, Fig. 2) (a) for Sn and (b) for P in Case AII where linearized ternary thermodynamic information and feeding flow are considered (CuSn6P0.5).

The calculated normalized c^i_{mix} profiles indicate positive macrosegregation at the outer boundary and negative one at the centre of the casting for Sn and P. As Fig. 2 shows, this is also observed in experimental measurements of the Sn distribution. However, since the P content in the simulated case was considered to be around 20 times higher than in the experiment, a validation of the P distribution is not possible up to now. It can be seen, that the negative macrosegregation for Sn is overestimated in the centre of the casting. A reason for that could be that less Sn is built into the solid phase due to the simplified thermodynamics. Generally it can be stated that the predicted macrosegregation for Sn and P of Case AII reflects the same trend because both alloying elements are enriched linearly during solidification due to the applied linear solidification approach.

Ternary Calculation using Splines and Considering Feeding Flow (Case B)

Since a simulation with linearized thermodynamic functions does not reflect the correct microsegregation evolution (at least not correct for Sn with $f_l \leq 0.5$), the use of splines of third order to approximate T_L, $\tilde{c}^{Sn}_c$, and $\tilde{c}^P_c$ in the concentration range of interest was tested. Coupling the thermodynamics to the multiphase volume averaging code this way was done and tested with considering feeding inducted flow (Case B). After reaching sufficiently small residuals at the beginning of the simulation, the residuals suddenly start to diverge and the calculation stopped before a complete steady-state was reached. Fig. 8 shows the corresponding liquid con-

centration for Sn and P shortly before crashing of the simulation. The lower part of the figures reflects that steady-state is still missing. However, the results above the dotted lines are close to steady-state. In Fig. 9, c_l^i is taken along the dotted line and plotted as function of f_l. Note that the volume averaged process simulation predicts that the Sn content in the interdendritic liquid decreases with decreasing f_l. This is obvious in Fig. 9, but can also be seen in the zoomed in picture of Fig. 8.

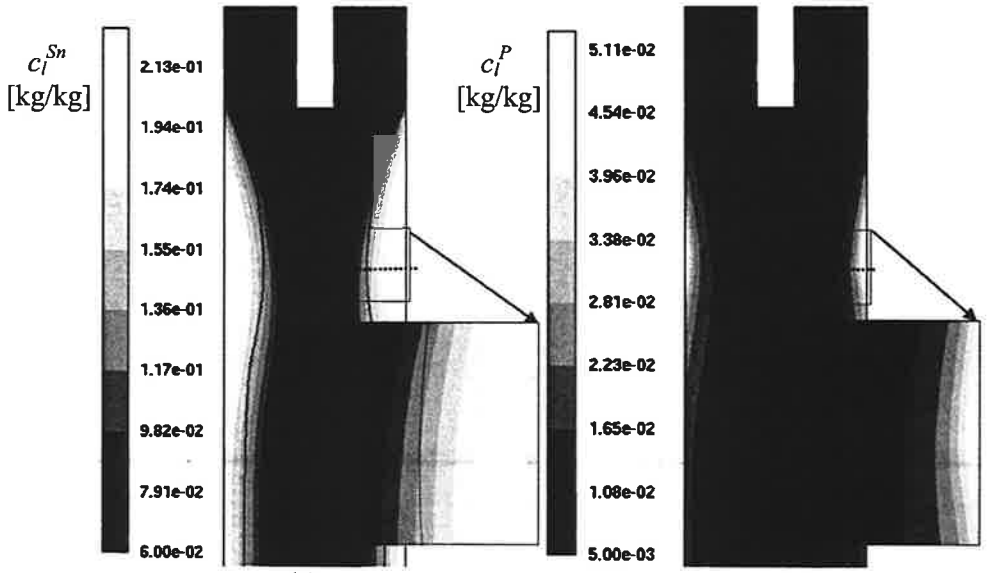

Figure 8: c_l^i (Sn left, P right) calculated with the two-phase volume averaging simulation for CuSn6P0.5 by using splines of the third order to approximate T_L, $\tilde{c}_c^{Sn}$, and $\tilde{c}_c^{P}$.

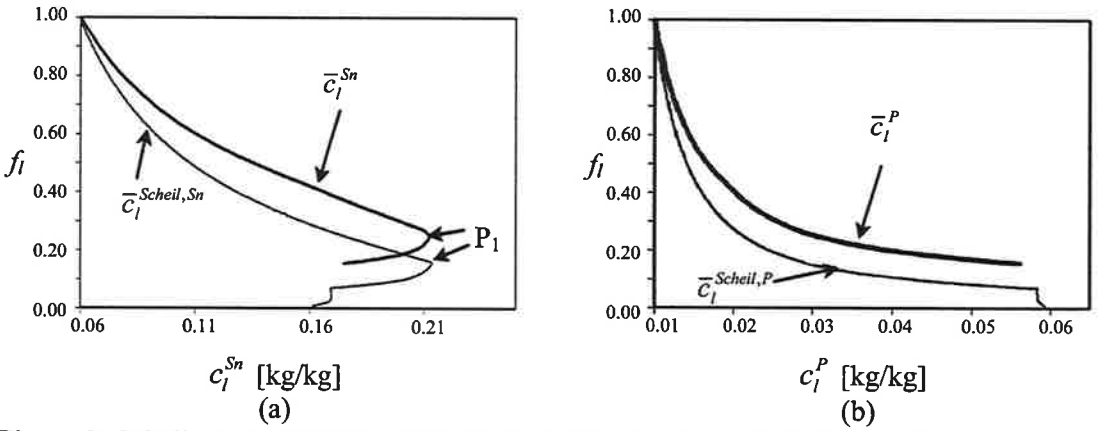

Figure 9: Scheil curve calculated with Thermo-Calc (database CuSnII, gray line) compared to the f_l as function of c_l^{Sn} and c_l^P calculated with the two-phase volume averaging simulation for CuSn6P0.5 (black line). Curves are taken at the dotted line in Fig. 7.

This decreasing Sn content is caused by the fact that the solubility of the β- and γ- solid is higher compared with the α-solid, and so crossing the corresponding peritectic grooves result in an increasing integration of Sn in the growing solids. In contrast to that the P content steadily increases in the interdendritic melt. In Fig. 9 it can be seen that the f_l versus c_l^{Sn} and c_l^P curves are shifted to lower liquid fractions compared to the ternary Scheil curves. A reason for that

could be the consideration of the feeding induced flow. A quantitative proof of this statement is ongoing.

Summary

Two different models are presented and discussed for ternary solidification simulation. The thermodynamic of Cu-Sn-P is included (i) by using linearized phase diagram information for a case without taking feeding flow into account (Case AI) and one with including it (Case AII), and (ii) by using splines for a case with feeding flow (Case B).

Concluding the following is stated:

- Ternary simulation based on a linear solidification path is a fast, first approach but leads to deviations from thermodynamic predictions at low volume fraction liquid.
- Ternary simulation based on nonlinear splines enables the modeling of strong concentration changes but is still under development.

Based on the liquid and solid concentration of the calculation on the one hand microsegregation and macrosegregation can be predicted for the solidified strand. Although calculations with nonlinear splines are still challenging and show rather high calculation costs, further work will be performed to ensure enhanced inclusion of higher order thermodynamics for the next future.

Acknowledgement

This work was financially supported by the Austria Christian-Doppler Society (CDG) and Wieland Werke for which the authors kindly acknowledge.

References

1. A. Ludwig, M. Gruber-Pretzler, M. Wu, A. Kuhn, J. Riedle, *Fluid Dyn. Mater. Proc.*, 1, 4(2006), 285-300.
2. L. Kaufman, H. Bernstein, *Computer Calculation of Phase Diagrams with Special Reference to Refractory Metals*, New York: Academic Press(1970).
3. J.O. Andersson, T. Helander, L. Höglund, P. Shi, B. Sundman, *Calphad*, 26(2002), 273-312.
4. B. Sundman, B. Jansson, J.O. Andersson, *Calphad*, 9(1985), 153-190.
5. W.Q. Jie, R. Zhang, Z. He, *Mater. Sci. Eng.* A. 413-414(2005), 497-503.
6. T. Kraft, M. Rettenmayr, H.E. Exner, *Progress in Mater. Sci.*, 42(1997), 277-286.
7. D. Larouche, *Computer Coupling of Phase Diagrams and Thermochemistry*, 31(2007), 490-504.
8. D. G. Eskin, Q. Du, R. Nadella, A.N. Turchin, L. Kagerman, *Proc. of the 5th Dec. Int. Conf. on Solid. Proc.*(2007), 437-441.
9. M. Gruber-Pretzler, *PhD Theses*, University of Leoben(2008).
10. A. Ludwig, M. Gruber-Pretzler, F. Mayer, A. Ishmurzin, M. Wu, *Mat. Sci. Eng. A,* 413-414(2005), 485-489.
11. A. Ludwig, A. Ishmurzin, M. Gruber-Pretzler, F. Mayer, M. Wu, *Proceedings of the 5th Dec. Int. Conf. on Solid. Proc.*(2007), 493-496.
12. A. Ishmurzin, M. Gruber-Pretzler, F. Mayer, L. Könözsy, M. Wu, A. Ludwig, *IJMR*, 99(2008), 618-25.
13. A. Ludwig, M. Wu, *Metall. Mater. Trans.*, 33A(2002), pp. 3673.
14. M. Wu, *Habilitationsschrift*, University of Leoben(2007).
15. M. Wu, A. Ludwig, *Metall. Mater. Trans.*, 37A(2006), pp. 1613.
16. M. Wu, A. Ludwig, *Metall. Mater. Trans.*, 38A(2007), pp. 1465.
17 G. Effenberg, S. Ilyenko, *Landolt-Börnstein-Group IV Physical Chemisty*(2007), 355-367.